

Ion Radial Transport due to a Non-Uniform Electrostatic Potential in a Magnetic Mirror

KATANUMA Isao, SAIMARU Hiroshi, TATEMATSU Yoshinori, SAITO Teruo,
ISHII Kameo and CHO Teruji

Plasma Research Center, University of Tsukuba, Tsukuba 305-8577, Japan

(Received: 9 December 2003 / Accepted: 20 March 2004)

Abstract

The density around the thermal barrier in a tandem mirror is sustained to be much lower than that in the central cell experimentally, which suggests that the ions trapped in the thermal barrier potential escape from there rapidly.

Although the mechanism of radial loss of ions trapped in the axisymmetric end-mirror cells are unknown in the present tandem mirror experiment, the electrostatic potential has been measured to be not axisymmetric around the plug region.

Because a numerical calculation reveals that the ion orbits trapped in a non-axisymmetric electrostatic potential (with many high m azimuthal modes around the plug) have a chaotic behavior, the non-axisymmetric electrostatic potential can be a candidate of a large ion radial loss in the axisymmetric end-mirror cells.

Keywords:

particle orbits, chaotic orbits, non-uniform electrostatic potential, mirror, magnetic mirror

1. Introduction

Although the tandem mirrors have revealed several unknown mechanisms on plasma confinement in an open-ended magnetically confinement system, one of a major purpose of a tandem mirror to find the mechanism of the plug and thermal barrier potential formations has been solved by ourselves theoretically [1,2,3].

Figure 1 shows the numerical results of a Monte-Carlo simulation [1,2,3], where the following electron population and ion loss are required to obtain the results, i.e., the population of electrons with two temperatures (cold component T_{ec} and warm component T_{ew}) in the central cell for the deep thermal barrier potential formation, where the standard notations are used through this paper, a non-Maxwellian electrons with different $T_{e\parallel}$ and $T_{e\perp}$ in the plug region for a plug potential formation, and the rapid loss of ions trapped in the thermal barrier potential for the thermal barrier potential formation. The parameters adopted in Fig. 1 are not contradictory to the observations in the experiments of the plug potential formation in the GAMMA10 tandem mirror [4].

It is seen that the plug potential has a sufficient height to confine the ions from the central cell because $e(\phi_p - \phi_i)/T_i \approx 3.2$ in Fig. 1(a) and $e(\phi_p - \phi_i)/T_i \approx 2.4$ in Fig. 1(b), while ion density gradually decreases from $z = z_i$ toward $z = z_m$, which clearly satisfies the relation $n_i(z_i) \gg n_i(z_b) \geq n_i(z_p)$,

where z_p is the axial position at local maximum of electrostatic potential.

Electrostatic potential and ion density axial profiles

$$T_{ec} / T_i = 0.2, \quad T_{ew} / T_i = 2$$

$$T_{e\perp} / T_{e\parallel} = 200, \quad n_{ew} / (n_{ec} + n_{ew}) = 0.04$$

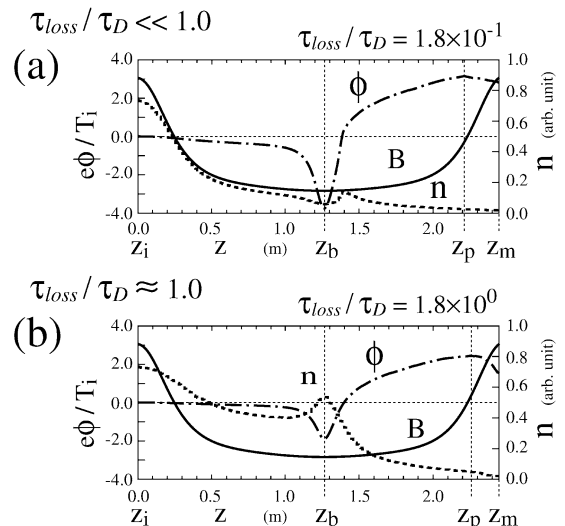


Fig. 1 Numerically obtained axial profiles of electrostatic potential and ion density in the plug/thermal barrier (end-mirror) cell. Here (a) is the case $\tau_{loss}/\tau_D = 1.8 \times 10^{-1}$ and (b) is $\tau_{loss}/\tau_D = 1.8 \times 10^0$.

Corresponding author's e-mail: katanuma@prc.tsukuba.ac.jp

The ion loss time is assumed as $\tau_{loss}/\tau_D = 0.18$ in Fig. 1(a) and $\tau_{loss}/\tau_D = 1.8$ in Fig. 1(b), where τ_D is the Coulomb deflection times defined as $\tau_D \equiv \sqrt{m_i} T_i^{3/2} / (\sqrt{2} \pi n_0 e^4 \ln \Lambda_{ii})$.

Radial loss of ions, which is included in this numerical calculation as τ_{loss} , is necessary for steady state potential formation. In GAMMA10, the plug/barrier potential structure can be sustained during 150 msec and no ion filling into the thermal barrier region has been observed [5]. This strongly suggests the existence of an ion radial loss in the plug/thermal barrier cell in GAMMA10 experiments.

The open-ended system such as a tandem mirror does not have any magnetic surfaces, which is a different point from a closed system such as a tokamak. The cross section of a magnetic flux tube, therefore, does not necessarily coincide with the equi-contour surface of an electrostatic potential, where experimental data on the equi-contour surfaces will be shown later in this paper.

The shape of a magnetic flux tube and the magnitude of an electrostatic potential on the flux tube are illustrated in Fig. 2, where the GAMMA10 has an axisymmetric magnetic field in the end-mirror cell in Fig. 2(a). Because a plug potential is created by electron cyclotron resonance heating (ECRH) mainly the cross section of equi-contour of the electrostatic potential around $z = z_p$ is generally non-axisymmetric as seen in Fig. 2(b) depending on the radiation pattern of μ -wave and the absorption rate at the resonance surface around [5].

2. Ion radial loss in the thermal barrier region

In order to investigate an ion radial loss due to a non-axisymmetric electrostatic potential we adopt a model of electrostatic potential profile in Eq. (1), where the axial profile on axis ($\psi = 0$) is shown in Fig. 3.

$$\begin{aligned} \phi(\psi, \theta, z) &= \left[\phi_p + \tilde{\phi} \frac{\psi}{\psi_0} \sum_m \cos(m\theta + \xi_m) \right] g(z) \\ &\times \exp\left(-\frac{\psi}{\psi_0}\right) + \phi_B \exp\left(-\frac{\psi}{\psi_0}\right); \text{ for } z \geq z_b, \\ \phi(\psi, \theta, z) &= \phi_i \frac{(z - z_b)^2}{(z_i - z_b)^2} \exp\left(-\frac{\psi}{\psi_0}\right) \\ &+ \phi_B \exp\left(-\frac{\psi}{\psi_0}\right); \text{ for } z < z_b. \end{aligned} \quad (1)$$

Here $g(z) = -A(z - a)(z - b)^2$ with $a > b$, where $z = z_b = b$ is the coordinate at the thermal barrier and $z = z_p = (2a + b)/3$ is the coordinate at the plug, A is a normalization factor to be $g(z_p) = 1$, i.e., $A = 3^3/(4(a - b)^3)$. The flux coordinates (ψ , θ , z) are adopted in Eq. (1), where magnetic field is represented by $\mathbf{B} = \nabla\psi \times \nabla\theta$. A long thin approximation to the magnetic field lines is assumed to calculate magnetic field lines and its curvatures at arbitrary point (ψ , θ , z) in order to trace ion

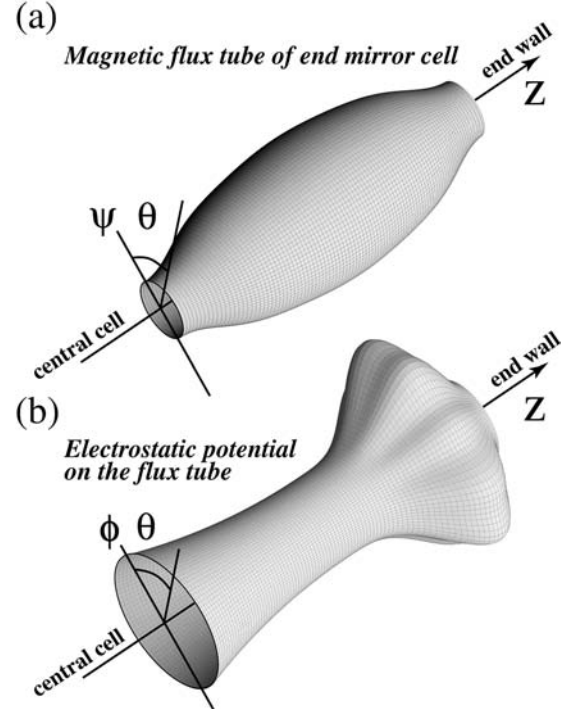


Fig. 2 Magnetic flux tube of the plug/thermal barrier cell of GAMMA10 (a), and the magnitude of an electrostatic potential on the magnetic flux tube (b).

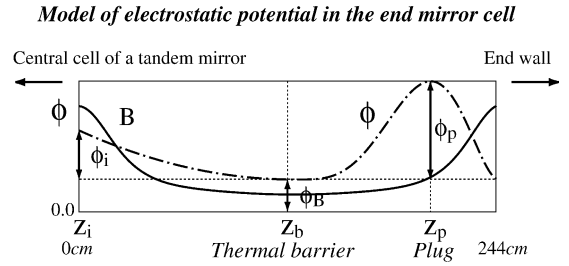


Fig. 3 Model of electrostatic potential axial profile used in the calculation of ion orbits.

orbits in the following [6,7,8]. The half width of electrostatic potential ψ_0 in Eq. (1) is given as $\psi_0 = 1/2B(z = z_b) \times 10^2$ (Gcm²).

We are interested in the ion radial transport without Coulomb collisions so that only the ion orbits are traced in the end-mirror cell of GAMMA10. Ions are distributed at $t = 0$ at ($r = 5\text{cm}$, $z = z_b$) with the same energy of 100eV but different pitch angles from 0 to $\pi/2$.

Figure 4 shows the results of ion orbit calculation when only $m = 3$ perturbation is added to the axisymmetric plug potential in Eq. (1). The ratio $\tilde{\phi}/\phi_p$ is the perturbation amplitude divided by the axisymmetric amplitude of electrostatic potential (see Eq. (1) and Fig. 3). A large amplitude of $m = 3$ perturbation exists at $z = z_p$ in Fig. 4, where $e\phi_B/T_i = 1.5$. Figure 4(b) is the Poincare map at $z = z_b$ of ion orbits, where each dot represents a locus of test ions at the position passing through $z = z_b$ until $t = 5\text{msec}$. Even if

large ion drifts from $r = 5\text{cm}$ initial radial position exist, many ions have regular orbits. As long as a single m mode perturbation is added to the axisymmetric electrostatic potential around plug region $z = z_p$, almost all the ion orbits are regular.

On the other hand, the case of $\sum_m \Rightarrow \sum_{m=3}^{11}$ in Eq. (1) is plotted in Fig. 5. Here $\tilde{\phi}/\phi_p = 0.08$ per each perturbed m mode was added to the axisymmetric electrostatic potential $z \geq z_b$. Equi-contour surfaces of electrostatic potential at $z = z_p$ is plotted in Fig. 5(a), where $e\phi_B/T_i = 1.5$. The small irregular perturbations are seen in the equi-contour surfaces of potential in Fig. 5(a). The Poincare map at $z = z_b$ of ion orbits in the electrostatic potential of Fig. 5(a) is plotted in Fig. 5(b) at $t = 5\text{msec}$. Under this electrostatic potential profile many ions have irregular motion, i.e., chaotic orbits.

Ion orbits become chaotic under the existing of many mode perturbations of electrostatic potential around plug as seen in Fig. 5. The mean square displacement $\langle \Delta r^2 \rangle$ of ions is defined as

$$\langle \Delta r^2 \rangle \equiv \sum_{i=1}^N \frac{(r_i - r_0)^2}{N}, \quad r_0 \equiv \sum_{i=1}^N \frac{r_i}{N}. \quad (2)$$

Here r_i is the i th test ion radial position mapped at $z = z_b$. If ions have a random walk process, $\langle \Delta r^2 \rangle$ will be proportional to time t , in the case of which ion radial diffusion coefficient D can be defined as $D \equiv \langle \Delta r^2 \rangle / t$.

Although it is known that ions under a chaotic motion have a sub-diffusion process but not a simple diffusion process, it is interesting to investigate the ion diffusion under the electrostatic potential profile such as that in Fig. 5(a). In GAMMA10 we estimate that the ion radial diffusion in the thermal barrier region is roughly $D \geq 5 \times 10^3 \text{cm}^2/\text{sec}$, because collisional filling time of passing ions with $n_i \approx 10^{11}/\text{cm}^3$ and $T_i \approx 100\text{eV}$ into the thermal barrier is about several *msec* and so the radial diffusion time of ions trapped there is comparable to the collision filling time in the steady state, i.e., $D \approx \frac{(5 \text{cm}^2)}{5 \times 10^{-3} \text{sec}}$. Now we introduce a target diffusion coefficient $D_{\text{target}} = 5 \times 10^3 \text{cm}^2/\text{sec}$. That is, the purpose here is to make clear that how much amplitude of electrostatic perturbation causes an ion radial diffusion of D_{target} .

The radial diffusion coefficient measured by a mean square displacement of test ions in the electrostatic potential in Fig. 4(a) is about $10^2 \text{cm}^2/\text{sec}$ which is much smaller than D_{target} . The case that many modes perturbation is added to an axisymmetric electrostatic potential such as in Fig. 5(a), therefore, is calculated hereafter.

Figure 6 displays the ion mean radial displacement in the electrostatic potential where the perturbations from $m = 3$ to 11 modes were added to the axisymmetric electrostatic potential in Eq. (1). Here $e\phi_B/T_i = 0.5$ is chosen, in which ions drift roughly $2\pi/9$ in the θ -direction per one bounce axial motion. Many ions with different pitch angles resonate with the electrostatic perturbation and their motion become chaotic as seen in Fig. 5(b). It is found that the ion radial diffusion coefficient satisfies $D \geq D_{\text{target}}$ when the ratio $\tilde{\phi}/\phi_p \geq 0.08$ in

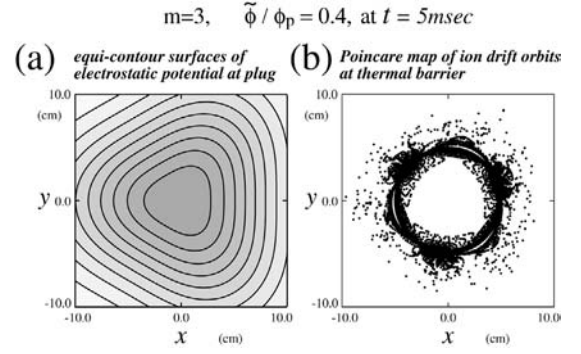


Fig. 4 Equi-potential surfaces at z_p in the case of which an $m = 3$ perturbation is added (a), and a Poincare map at $z = z_b$ of ion orbits (b).

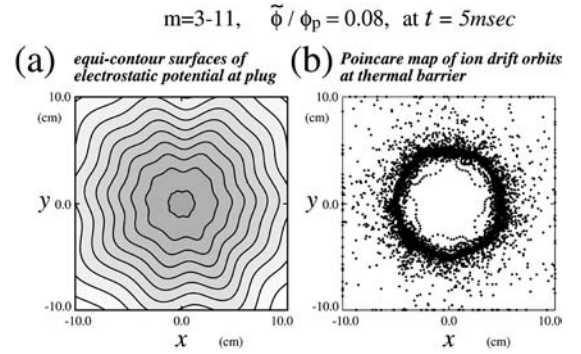


Fig. 5 Equi-potential surfaces at z_p in the case of which the perturbations from $m = 3$ to $m = 11$ are added to an axisymmetric electrostatic potential (a), and a Poincare map at $z = z_b$ of ion orbits (b).

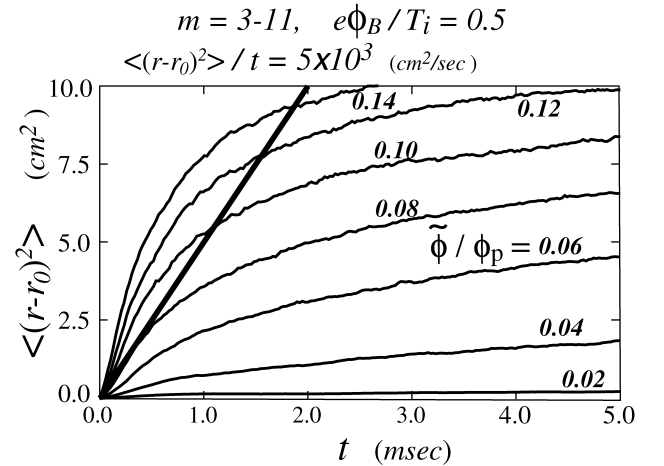


Fig. 6 Time evolution of test ion mean square displacements.

Fig. 6(a).

The electrostatic potential at the thermal barrier $z = z_b$ is measured by a beam probe in GAMMA10 [5,6], where Fig. 7 is a latest result of GAMMA10. The radial profile of the electrostatic potential depends strongly on the radiation pattern of externally injected μ -wave for ECRH at $\omega = \omega_{ce}$ fundamental resonance surface around the plug $z = z_p$. By

